ACS APPLIED MATERIALS & INTERFACES

RESEARCH ARTICLE

www.acsami.org

A Novel Tunable Green- to Yellow-Emitting β-YFS:Ce^{3+} Phosphor for Solid-State Lighting

Yun-Chen Wu,[†] De-Yin Wang,[†] Teng-Ming Chen,*[,†] Chi-Shen Lee,[‡] Kuo-Ju Chen,[§] and Hao-chung Kuo[§]

[†]Phosphors Research Laboratory, Department of Applied Chemistry and Institute of Molecular Science, [‡]Solid-State Inorganic Applied Material Laboratory, Department of Applied Chemistry and Institute of Molecular Science, and [§]Semiconductor Laser Technology Laboratory, Department of Photonics, National Chiao Tung University, Hsinchu 30010, Taiwan

ABSTRACT: A Ce^{3+}-activated fluorosulfide phosphor (β-YFS:Ce^{3+}) was synthesized by solid-state reaction in a sealed tube. The crystal structure has been refined from the XRD profiles and there are two different crystallographic rare earth sites, namely, Y(1) and Y(2), where the Ce^{3+} ions occupied. The emission band with a maximum at 495 nm of β-$Y_{0.99}Ce_{0.01}FS$ phosphor was characterized by the 4f-5d transitions of Ce^{3+} ion. With increasing Ce^{3+} concentration, the emission variations were observed from 495 to 547 nm. When β-YFS:Ce^{3+} phosphors were utilized to incorporate with n-UV/blue chip, greenish-white light with color rendering index of 65−77 were obtained. The results indicate that the tunable green- to yellow-emitting β-YFS:Ce^{3+} can serve as a potential phosphor for incorporation in fabrication for solid-state lighting. The preparation, spectroscopic characterization, quantum efficiency, thermal-quenching behavior, and related LED device data are also presented.

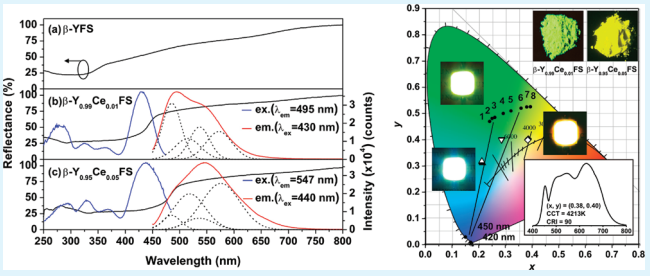

KEYWORDS: β-YFS, Ce^{3+}, fluorosulfide, phosphor, emission-tunable, LED

INTRODUCTION

Commercial white light-emitting diodes (LED) usually comprise binary complementary color system, viz., a high-performance blue-emtting LED chip and a yellow-emitting $(Y,Gd)_3(Al,Ga)_5O_{12}:Ce^{3+}$ (YAG:Ce) phosphor/resin mixture layer.[1] This type of white LED has attracted much attention because of its merits of long-term operational lifetime, energy savings, compactness, environmental friendliness, and high efficiency.[2,3] However, it is also characterized as cool white light because of its high correlated color temperature (CCT) of >8000 K, and poor color rendering index (CRI, *Ra*) of 75.[4] The mentioned drawbacks restrict the white LED application in general and medical lighting. Recently, several white LED modules fabricated using near-ultraviolet (n-UV) (380−420 nm) chip coupled with a blend of tunable green-to-yellow- and red-emitting phosphor.[5,6] They exhibited surprisingly favorable properties, including tunable CCTs, tunable CIE chromaticity coordinates, and excellent CRI values. Accordingly, it is important to develop new green- or yellow-emitting phosphor for n-UV LED application. The Ce^{3+} emission usually consists of a broad band due to the parity allowed characteristics of the transition between the lowest crystal field components 5d excited state and the 4f ground state ($^2F_{7/2}$ and $^2F_{5/2}$), and can be varied from ultraviolet to yellow in its emitting color, depending on the different host lattices. Many Ce^{3+}-activated green- to yellow-emitting phosphors used for n-UV and blue chip have been reported, including $(Sr,Ca)_3(Al,Si)O_4(F,O):Ce^{3+}$,[5] $(Sr,Ba)_3(Al,Ga)O_4F:Ce^{3+}$,[6−8] $CaSc_2O_4:Ce^{3+}$,[9] $Ca_3Sc_2Si_3O_{12}:Ce^{3+}$,[10,11] $(Ca,Sr)S:Ce^{3+}$.[12]

The β-YFS crystal was first reported by Rysanek et al.[13] as a new halogensulfide material. To the best of our knowledge, the luminescence properties of β-YFS:Ce^{3+} phosphor has not yet been reported in literature. In this paper, we investigated the crystal structure of β-YFS lattice and reported the luminescent properties of Ce^{3+}-doped β-YFS. This new phosphor can be excited by light in n-UV to blue region and shows tunable green to yellow emission. In addition, the LED device using different Ce^{3+} concentration β-YFS phosphors with n-UV or blue chip were fabricated to demonstrate the applicability of β-YFS phosphor as a color conversion material.

EXPERIMENTAL SECTION

Materials. Polycrystalline powder samples of β-$Y_{1-x}Ce_xFS$ were prepared by solid-state reactions with YF_3 (Aldrich), Y_2S_3 (Alfa), Ce_2S_3 (Alfa), and S (Aldrich) as raw materials. The stoichiometric amounts of the starting materials were thoroughly mixed and loaded into a Al_2O_3 tubing, which was transferred into a vertically positioned quartz ampule, fully evacuated to 10^{-3} Torr and sealed off. The quartz ampule was heated to 1150−1200 °C for 8−12 h and then cooled slowly to room temperature. The obtained product was then annealed at 900 °C for 4 h under a 5% H_2/Ar atmosphere.

Characterization. The phase purity of the samples was analyzed by powder X-ray diffraction (XRD) using a Bruker AXS D8 advanced automatic diffractometer with Cu Kα radiation (λ = 1.5418 Å, 40 kV × 40 mA). The powder diffraction data were subjected to perform a computer software General Structure Analysis System (GSAS) package.[14] Refined structure parameters comprised overall scale factors, lattice parameters,

Received: May 31, 2011
Accepted: July 6, 2011
Published: July 06, 2011

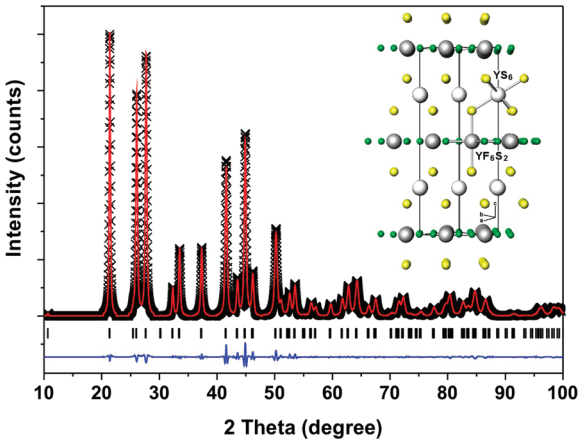

Figure 1. Rietveld refinement results of β-$Y_{0.99}Ce_{0.01}FS$ using X-ray powder diffraction data and the structure parameters. Observed intensities (cross), calculated patterns (red line), Bragg positions (|), and difference plot (blue line). The inset shows the schematic unit cell crystal structure of β-(Y,Ce)FS and coordination environment around YS_6 and YF_6S_2. White, gray, green, and yellow spherical balls represents Y(1)/Ce, Y(2)/Ce, F, and S atoms, respectively.

and fractional coordinates. The diffuse reflection spectra were measured with a Hitachi 3010 double-beam ultraviolet−visible (UV−vis) spectrometer (Hitachi Co., Tokyo, Japan) equipped with a ø60-mm integrating sphere. The photoluminescence (PL) and photoluminescence excitation (PLE) spectra were recorded with a Spex Fluorolog-3 spectrofluorometer (Jobin Yvon Inc./specx) equipped with a 450 W Xe lamp and analyzed by a Jobin-Yvon spectrometer HR460 with multichannel charge-coupled device detector. The Commission Internationale de l'Eclairage (CIE) chromaticity coordinates were determined by a Laiko DT-100 color analyzer equipped with a CCD detector (Laiko Co., Tokyo, Japan). The pc-WLEDs devices were fabricated using commercial blue InGaN-based LEDs (λ_{max} = 420 and 450 nm) with an intimate mixture of as-synthesized phosphors and silicone resin. Electroluminescence spectra were recorded at a forward-current and measured by using a SphereOptics integrating sphere with LED measurement starter packages (Onset, Inc.).

RESULTS AND DISCUSSION

Structural Characterizations and Crystallographic Parameters of the β-$Y_{0.99}Ce_{0.01}FS$ Phosphor. Figure 1 shows the results of the data collection and structure refinements for β-$Y_{0.99}Ce_{0.01}FS$. The single crystal structure data of β-YFS[15] (ICSD No. 89548) was performed as a starting reference for β-phase fluorosulfides to approach a dependable approximation of the actual crystal structure. The final converged weighted-profile of R_p = 2.15%, R_{wp} = 5.52%, χ^2 = 0.29 show the single phase with no unidentified diffraction peaks from impurity (Table 1). For β-$Y_{0.99}Ce_{0.01}FS$, the lattice constants were examined to be $a = b$ = 4.0523(1) Å, c = 16.6812(4) Å, and the cell volume was determined as 237.23(2) Å^3. The bond valence sums (BVS) shows Y(1) with 2.92 and Y(2) with 2.86, which suggest that Ce substitution in present experiment can be maintained in the β-YFS lattice structure (Table 2). The β-$Y_{0.99}Ce_{0.01}FS$ synthesized in this study was found to crystallize hexagonally in $P6_3/mmc$ space group (No. 194) with Z = 4. In the crystal structure of β-YFS, there are two crystallographically distinctive sites for Y atoms. The Y(1) atom occupies the 2*a* position site in the center of octahedral YS_6 polyhedron (CN = 6) and Y(2) atom occupies the 2*c* position site in the center of hexagonal bipyramidal YS_2F_6 polyhedron (CN = 8). The Ce^{3+} ions would experience two different crystal field splitting due to the different coordination environments in $Y(1)S_6$ and YS_2F_6 polyhedra and this part is to be discussed later. Furthermore, the 2*b* and 2*d* sites are fully occupied by F atoms and the 4f site is fully occupied by S atoms. The structure of β-YFS can be described as an ordered intergrowth $Y(1)S_6/Y(2)S_2F_6$ polyhedra layer structure similar to LuFS ($R\bar{3}m$, No.166),[15] composing of one layer of $Y(1)S_6$ and one layer of $Y(2)F_6$ along the *c*-axis repeat.

Table 1. Structural Parameters of β-$Y_{0.99}Ce_{0.01}FS$ of Rietveld Refinement from XRD Data at Room Temperature

formula	β-$Y_{0.99}Ce_{0.01}FS$
cryst syst	hexagonal, $P6_3/nmc$ (No. 194)
units, Z	4
a (Å)	4.0523(1)
b (Å)	4.0523(1)
c (Å)	16.6812(4)
V (Å^3)	237.23(1)
α (deg)	90
β (deg)	90
γ (deg)	120
R_{wp} (%)	5.52
R_p (%)	2.15
χ^2	0.29

atom	Wyck.	x/a	y/b	z/c	U (Å^2)
Y1	2*a*	0	0	0	0.0074(1)
Y2	2*c*	0.33	0.67	0.25	0.0016(1)
S	4*f*	0.33	0.67	0.0862(1)	0.0292(1)
F1	2*b*	0	0	0.25	0.0186(2)
F2	2*d*	0.33	0.67	0.75	0.0414(1)

Table 2. Selected Bond Distances and Bond Valence Sums of β-$Y_{0.99}Ce_{0.01}FS$ at Room Temperature

β-$Y_{0.99}Ce_{0.01}FS$ bond distance (Å)		BVS	
(Y1/Ce)−S	2.74653(5) (4×) 2.74653(5) (2×)	Y1	2.92
(Y2/Ce)−S	2.73187(7) (2×)	Y2	2.86
(Y2/Ce)−F1	2.33974(6) (2×) 2.33939(6) (1×)		
(Y2/Ce)−F2	2.33974(6) (2×) 2.33939(6) (1×)		

Spectroscopic Characterizations of β-$Y_{1-x}Ce_xFS$ Phosphor. Figure 2 shows the diffuse reflection spectra of β-YFS, β-$Y_{0.99}Ce_{0.01}FS$, and β-$Y_{0.95}Ce_{0.05}FS$. The β-YFS host shows energy absorption in the 250−375 nm region. The fundamental band gap energy (absorption edge) of β-YFS host was calculated to be approximately 3.2 eV by extrapolating from the Kubelka−Munk absorption coefficient-related spectrum.[16]

$$\frac{K}{S} = \frac{(1-R)^2}{2R} \quad (1)$$

where K represents the absorption coefficient; S represents the scattering coefficient; R represents the reflectivity. When 1% Ce^{3+} was induced into the β-YFS host lattice, an apparent reduction of reflectance from 250 to 460 nm was observed. With

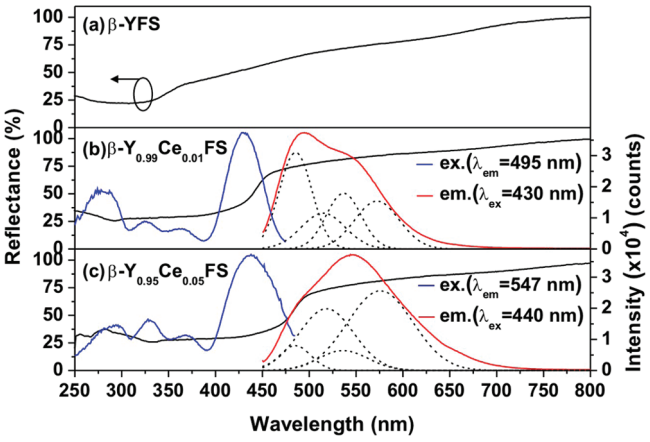

Figure 2. (a) Diffuse reflection spectrum of β-YFS. (b) Diffuse reflection spectrum, PLE/PL spectra, and the PL deconvolution of β-$Y_{0.99}Ce_{0.01}FS$. (c) Diffuse reflection spectrum, PLE/PL spectra, and the PL deconvolution of β-$Y_{0.95}Ce_{0.05}FS$.

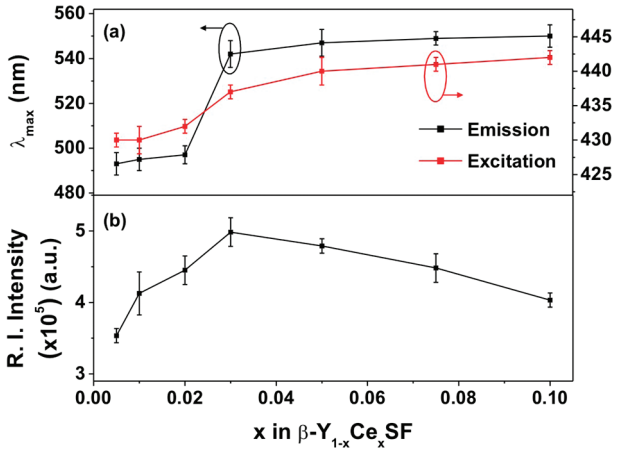

Figure 3. (a) Comparison of the maximum wavelength for β-$Y_{1-x}Ce_xFS$. (b) Relative integrated intensity as a function of x in β-$Y_{1-x}Ce_xFS$.

further increasing the Ce^{3+} concentration to 5%, the band edge extends to a longer wavelength side and the absorption is enhanced. The observed results suggest two different absorption pathways from UV to visible range, namely, one is caused by β-YFS host and the other is caused by the $4f^1 \rightarrow 4f^05d^1$ transitions of Ce^{3+} ion. As can be seen from the PLE spectra ofβ-YFS:Ce^{3+}, the PLE spectra show four excitation bands, meanwhile, it is found that the maximum of the excitation band shifts to the longer wavelength for higher Ce^{3+} concentration. That is, the maximum of the Ce^{3+} excitation band shifts from 430 nm for a sample with 1% Ce^{3+} to 440 nm for a sample with 5% Ce^{3+}. The PL spectrum of the β-$Y_{0.99}Ce_{0.01}FS$ shows an typical asymmetric feature of Ce^{3+} emission peaking at 495 nm, which can be ascribed to the $4f^05d^1 \rightarrow 4f^1$ transitions of Ce^{3+} ions. With increasing Ce^{3+} concentration, the Ce^{3+} emission changes from 495 nm for the sample with 1% Ce^{3+} to 540 nm for the sample with 5% Ce^{3+}. This may results from that Ce^{3+} occupy in different sites, viz, Y(1) and Y(2) sites in β-YFS lattice, and energy transfer between Ce^{3+} ions in the two different sites occurs with increasing Ce^{3+} concentration. In β-YFS lattice, it is consisted of two distinct coordination polyhedrons. The Y(1) site in YS_6 polyhedron experience a stronger bond covalency strength than the Y(2) site in YS_2F_6 polyhedron.[17,18] This suggest that the green component around 495 nm is originated from the substitution of Ce^{3+} ion for Y^{3+} ion in Y(2) site whereas the yellow component around 547 nm is in Y(1) site. Both of them show completely different emission energies from their respective nondegenerate 5d orbitals. By Gaussian deconvolution, the PL spectra of β-$Y_{0.99}Ce_{0.01}FS$ and β-$Y_{0.95}Ce_{0.05}FS$ can be decomposed into four Gaussian components, with peaks centering at 484 nm (20,661 cm^{-1}), 514 nm (19,455 cm^{-1}), 536 nm (18,657 cm^{-1}), and 572 nm (17,483 cm^{-1}) (Figure 2b dash line) and 485 nm (20619 cm^{-1}), 518 nm (19,305 cm^{-1}), 537 nm (18,622 cm^{-1}), and 576 nm (17,361 cm^{-1}) (Figure 2c dash line), respectively. These components can be ascribed to the contribution of the transitions from the lowest 5d excited state to the two $^2F_{7/2}$ and $^2F_{5/2}$ ground states in Y(1) and Y(2) sites. The values of spin−orbit coupling were calculated to be 2004 and 1972 cm^{-1} in β-$Y_{0.99}Ce_{0.01}FS$, 1997 and 1944 cm^{-1} in β-$Y_{0.95}Ce_{0.05}FS$ (usually ~2000 cm^{-1}). The deconvolution result also confirms an overall red shift changing on the spectral shape, which is because of the energy transfer from Ce^{3+} at Y(2) with higher energy to that of Y(1) with lower energy as the concentration of Ce^{3+} increased. As a whole, the covalency of the β-YFS materials, to some extent, are similar to that of sulfide phosphor, e.g., (Ca,Sr)S:Ce^{3+},[19] although much more number of fluoride anion coordinate to Ce^{3+} in Y(2) site. In comparison with the Ce^{3+} doped fluorides phosphors (e.g., YF_3:Ce^{3+}, CsY_2F_7:Ce^{3+} and $KLiYF_5$:Ce^{3+}),[20−22] the β-YFS:Ce^{3+} phosphors show a longer emission, which can be attributed to the incorporation of Ce−S bond generate a larger nephelauxetic effect than that of Ce−F bond. The PLE results exhibit that the β-YFS:Ce^{3+} matches well with the emission of n-UV; thus, β-YFS:Ce^{3+} has the potential as a promising candidate for solid-state lighting.

As shown in Figure 3, with an increase of the Ce^{3+} concentration x, the maximum emission wavelength slightly increases with a breaking point at $x \approx 0.025$, from which the emission peak red shifting slightly. In contrast, the maximum excitation wavelength almost remains the same. Meanwhile, the optimum Ce^{3+} concentration or so-called critical concentration (x_c) is found to be x = 0.03, from which it can be used for determining the concentration quenching caused by the energy transfer mechanisms, such as exchange interaction, radiation reabsorption, or multipole-multipole interaction.[23] The critical transfer distance (R_c) is described as following expression.[23−25]

$$R_c \approx 2\left(\frac{3V}{4\pi x_c N}\right)^{1/3} \quad (2)$$

where V represents the volume of unit cell; x_c represents critical concentration; and N represents the number of total Ce^{3+} sites in the unit cell. According to the crystal structure of β-YFS:Ce^{3+}, R_c was calculated to be ~15.57 Å. Because the exchange interaction takes place generally in forbidden transition (the R_c is typically ~5 Å) as well as the PLE and PL spectra do not overlap very well. Therefore, we can infer that the nonradiative concentration quenching among two nearest Ce^{3+} centers occurs via electric multipolar interactions based on the Dexter theory. Besides, energy transfer may happen from a percolating Ce^{3+} cluster to a killer centers.[24]

Quantum Efficiencies and Temperature-Dependent PL Properties. As seen in Figure 4, β-$Y_{0.95}Ce_{0.05}FS$ exhibits a thoroughly higher internal quantum efficiency (IQE) values than that of β-$Y_{0.99}Ce_{0.01}FS$ under the excitation region range from

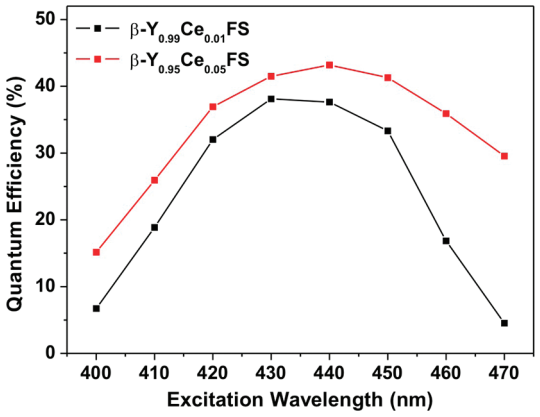

Figure 4. Dependence of the quantum efficiency on the excitation wavelength for β-$Y_{0.99}Ce_{0.01}FS$ and β-$Y_{0.95}Ce_{0.05}FS$.

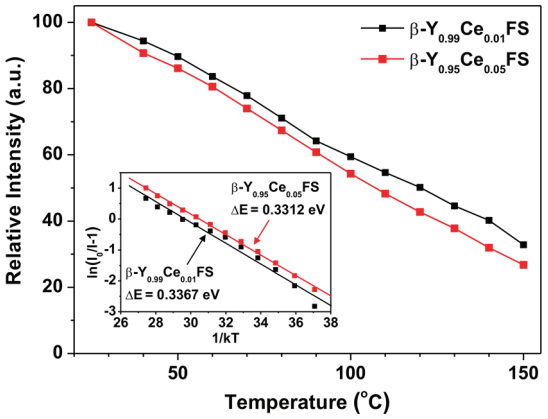

Figure 5. Temperature dependence of the PL integrated intensity for β-$Y_{0.99}Ce_{0.01}FS$ and β-$Y_{0.95}Ce_{0.05}FS$. The inset shows the activation energy of the β-$Y_{0.99}Ce_{0.01}FS$ and β-$Y_{0.95}Ce_{0.05}FS$ phosphors.

n-UV (400 nm) to blue region (470 nm). The notably low IQE values of the β-$Y_{0.99}Ce_{0.01}FS$ can be rationalized by the comparatively low absorption coefficients in β-$Y_{0.99}Ce_{0.01}FS$ sample when excited by different wavelengths. In addition, β-$Y_{0.95}Ce_{0.05}FS$ possesses higher integrated emission intensity, which results in the significant enhancement of the IQE value. The QE results show relative corresponding characteristics with the $4f^1 \rightarrow 4f^05d^1$ transitions observed on the PLE spectra. β-$Y_{0.99}Ce_{0.01}FS$ shows the QE of 31.97% under 420 nm and 33.39% under 450 nm excitation, compared to 37.1% and 41.31% in β-$Y_{0.95}Ce_{0.05}FS$, in which reflect the applicability for color conversion of white LED consisting of n-UV or blue chip.[26]

Figure 5 shows the temperature-dependent PL spectra of β-$Y_{0.99}Ce_{0.01}FS$ and β-$Y_{0.95}Ce_{0.05}FS$ in the range of 25 to 150 °C. As temperature increased, the PL intensity is found to be diminished rapidly as compared to that of the same sample observed at the room temperature. This may be results from that increasing temperature has increased the probability of ionization Ce^{3+} 5*d* electrons into the bottom of the conduction band.[27] In spite of the introduction of F ions into the sulfide host, the β-YFS:Ce^{3+} does not show a better thermal stability than that of the commodity CaS:Ce^{3+}. To verify the origin of temperature-dependent emission intensity $I(T)$, the activation energy (E_a) of the electrons excited from 4f states to the lowest 5d states of

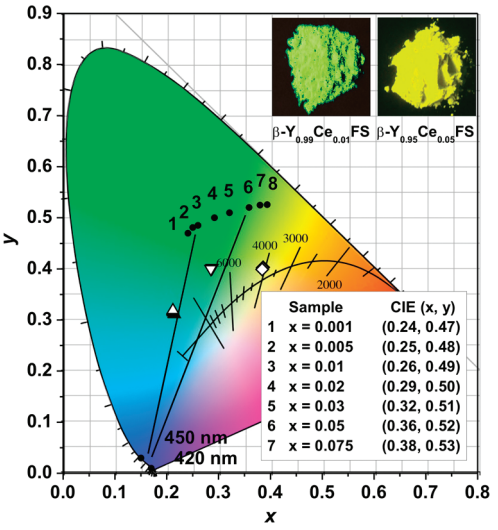

Figure 6. Variation in CIE chromaticity coordinates as a function of *x* in β-$Y_{1-x}Ce_xFS$ and the CIE coordinates of the fabricated LED are also presented. The inset shows β-$Y_{0.99}Ce_{0.01}FS$ and β-$Y_{0.95}Ce_{0.05}FS$ photos taken under 365 nm excitation.

Ce^{3+} can be described in following equation.[28]

$$I(T) = \frac{I_o}{1 + A\exp\left(-\frac{E_a}{kT}\right)} \quad (3)$$

where I_0 and I (T) represent the PL intensity at room temperature and testing temperature (25−150 °C), respectively; k represents Boltzmann constant. The E_a values for β-$Y_{0.99}Ce_{0.01}FS$ and β-$Y_{0.95}Ce_{0.05}FS$ were determined to be 0.3367 and 0.3312 eV, as shown in the inset in Figure 5. With increasing Ce^{3+} concentration, the thermal energy was found to decrease and could excite the 5d electron to the bottom of the conduction band more easily.

CIE chromaticity Coordinates and Performance of LED Device Based on β-YFS:Ce^{3+} Phosphor. Figure 6 shows the CIE chromaticity coordinates for the β-YFS:Ce^{3+} phosphors with different *x* values. The color hue can be tuned from green (point 1) to yellow (point 8), and the corresponding chromaticity coordinates (*x*, *y*) varying from (0.241, 0.47) to (0.409, 0.5) summarized in the inset Table. The inset photos show luminescence of β-$Y_{0.99}Ce_{0.01}FS$ and β-$Y_{0.95}Ce_{0.05}FS$ phosphors under excitation at 365 nm.

To demonstrate the potential of β-YFS:Ce^{3+} as a complementary color material for creating white light, β-$Y_{0.99}Ce_{0.01}FS$ and β-$Y_{0.95}Ce_{0.05}FS$ phosphors were used to fabricate LED devices with a 420 and 450 nm LED chip under different forward bias current in the range of 50−250 mA. Figure 7 shows the EL spectra of the LED device using β-$Y_{0.99}Ce_{0.01}FS$ and β-$Y_{0.95}Ce_{0.05}FS$ phosphors with n-UV or blue chip. The EL spectra show a n-UV band at around 420 nm, a blue band at around 450 nm, which belong to chip, and a green-emitting band corresponding to β-$Y_{0.99}Ce_{0.01}FS$ with the CIE coordinates ranging from (0.212−0.215, 0.319−0.311)and a yellow-emitting band corresponding to β-$Y_{0.95}Ce_{0.05}FS$ with the CIE coordinates ranging from (0.285−0.288, 0.4−0.402) under different current. The CRI values were obtained to be 65 and 77 for greenish-white light LED device. With the addition of proprietary red phosphor, the CRI value could be improved to 90. The corresponding CCT

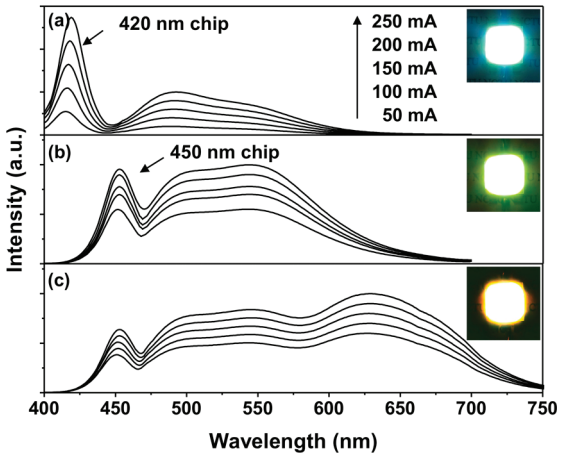

Figure 7. EL spectra of device using (a) β-$Y_{0.99}Ce_{0.01}FS$ + 420 nm chip, (b) β-$Y_{0.95}Ce_{0.05}FS$ + 450, and (c) β-$Y_{0.95}Ce_{0.05}FS$ + red phosphor +450 nm chip. The intensity increased as a function of current density. The insets show the corresponding LED device photograph.

and CIE were measured to be 4213K and (0.384−0.386, 0.399−0.403). The β-YFS:Ce^{3+} phosphors show their tunable suitability as a green or yellow emitter with the commercial chip. We anticipate that the observed CIE coordinates, CRI, and CCT values of the phosphor-converted LED device can be further improved by process optimization, such as heating control, particle size, and ratio of phosphor/resin.

CONCLUSION

In summary, we have synthesized the β-YFS:Ce^{3+} phosphors by a solid-state method in sealed quartz tube and investigated its overall luminescence performance (i.e., PL intensity, quantum efficiency, thermal-quenching behavior, and its application in LED fabrication). The results show that β-YFS:Ce^{3+} is excitable over a broad range from n-UV to blue light, and its emission can be adjusted from green to yellow by changing Ce^{3+} doping concentration. Applying a bled of β-YFS:Ce^{3+} and red phosphor on blue chip, we can obtain a warm white LED device with high CRI value of 90 and CCT value of 4213 K. With the interesting tunable emission property, β-YFS:Ce^{3+} phosphor has great application potential as a good color conversion material for solid state lighting.

AUTHOR INFORMATION

Corresponding Author

*E-mail: tmchen@mail.nctu.edu.tw.

ACKNOWLEDGMENT

This research was supported by National Science Council of Taiwan (ROC) under Contract NSC98-2113-M-009-005-MY3. We thank Dr. Ming-Yang Chung for assistance in the helpful suggestion.

REFERENCES

(1) Bachmann, V.; Ronda, C.; Meijerink, A. *Chem. Mater.* **2009**, *21*, 2077–2084.

(2) Mueller-Mach, R.; Mueller, G.; Krames, M. R.; Höppe, H. A.; Stadler, F.; Schnick, W.; Juestel, T.; Schmidt, P. *Phys. Status Solidi A* **2005**, *202*, 1727–1732.

(3) Krames, M. R.; Shchekin, O. B.; Mueller-Mach, R.; Mueller, G. O.; Zhou, L.; Harbers, G.; Craford, M. G. *J. Display Technol.* **2007**, *3* (2), 160–175.

(4) Setlur, A. A.; Heward, W. J.; Hannah, M. E.; Happek, U. *Chem. Mater.* **2008**, *20*, 6277–6283.

(5) Setlur, A. A.; Radkov, E. V.; Henderson, C. S.; Her, J. H.; Srivastava, A. M.; Karkada, N.; Kishore, M. S.; Kumar, N. P.; Aesram, D.; Deshpande, A.; Kolodin, B.; Grigorov, L. S.; Happek, U. *Chem. Mater.* **2010**, *22*, 4076–4082.

(6) Im, W. B.; Brinkley, S.; Hu, J.; Mikhailovsky, A.; DenBaars, S. P.; Seshadri, R. *Chem. Mater.* **2010**, *22*, 2842–2849.

(7) Chen, W. P.; Liang, H. B.; Han, B.; Zhong, J. P.; Su, Q. *J. Phys. Chem. C* **2009**, *113*, 17194–17199.

(8) Chen, W. P.; Liang, H. B.; Ni, H. Y.; He, P.; Su, Q. *J. Electrochem. Soc.* **2010**, *157*, J159–J163.

(9) Shimomura, Y.; Kurushima, T.; Kijima, N. *J. Electrochem. Soc.* **2007**, *154*, J234–J238.

(10) Shimomura, Y.; Honma, T.; Shigeiwa, M.; Akai, T.; Okamoto, K.; Kijima, N. *J. Electrochem. Soc.* **2007**, *154*, J35–J38.

(11) Shimomura, Y.; Kurushima, T.; Shigeiwa, M.; Kijima, N. *J. Electrochem. Soc.* **2008**, *155*, J45–J49.

(12) Jia, D. D.; Wang, X. J. *Opt. Mater.* **2007**, *30*, 375–379.

(13) Rysanek, P. N.; Lote, O. *Acta Crystallogr., Sect. B* **1973**, *29*, 1567–1569.

(14) Larson, A. C. Von Dreele, R. B. *General Structure Analysis System (GSAS)*; Los Alamos National Laboratory: Los Alamos, NM, 2004.

(15) Schleid, T. *Z. Anorg. Allg. Chem.* **1999**, *625*, 1700–1706.

(16) Aguirre, C. I.; Reguera, E.; Stein, A. *ACS Appl. Mater. Interfaces* **2010**, *2*, 3257–3262.

(17) Dorenbos, P. *Phys. Rev. B* **2002**, *65*, 235110–235116.

(18) Dorenbos, P. *J. Lumin.* **2003**, *105*, 117–119.

(19) Jia, D.; Wang, X. J. *Optics Mater.* **2007**, *30*, 375–379.

(20) Dorenbos, P. *J. Lumin.* **2000**, *91*, 155–176.

(21) Wang, Z. L.; Quan, Z. W.; Jia, P. Y.; Lin, C. K.; Luo, Y.; Fang, J.; Zhou, W.; O'Connor, C. J.; Lin, J. *Chem. Mater.* **2006**, *18*, 2030–2037.

(22) Li, C. X.; Liu, X. M.; Yang, P. P.; Zhang, C. M.; Lian, H. Z.; Lin, J. *J. Phys. Chem. C* **2008**, *112*, 2904–2910.

(23) Im, W. B.; Fellows, N. N.; DenBaars, S. P.; Seshadri, R.; Kim, Y. I. *Chem. Mater.* **2009**, *21*, 2957–2966.

(24) Kim, J. H.; Jung, K. Y. *J. Lumin.* **2011**, *131*, 1487–1491.

(25) Shang, M. M.; Li, G. G.; Kang, X. J.; Yang, D. M.; Geng, D. L.; Lin, J. *ACS Appl. Mater. Interfaces* **2011**, *3*, 2738–2746.

(26) Liu, W. R.; Huang, C. H.; Wu, C. P.; Chiu, Y. C.; Yeh, Y. T.; Chen, T. M. *J. Mater. Chem.* **2011**, *21*, 6869–6874.

(27) Wu, Y. C.; Chen, T. M.; Chiu, C. H.; Mo, C. N. *J. Electrochem. Soc.* **2010**, *157*, J342–J346.

(28) Xie, R. J.; Hirosaki, N.; Kimura, N.; Sakuma, K.; Mitomo, M. *Appl. Phys. Lett.* **2007**, *90*, 191101–191103.